CO_2 hydrogenation over Ru hydrotalcite-derived catalysts

Alexander Misol, Ilenia Giarnieri, Francesca Ospitali, Adriana Ballarini, José Jiménez-Jiménez, Enrique Rodríguez-Castellón, Francisco Martín Labajos, Giuseppe Fornasari, Patricia Benito

PII: S0920-5861(23)00386-3

DOI: https://doi.org/10.1016/j.cattod.2023.114362

Reference: CATTOD114362

To appear in: *Catalysis Today*

Received date: 30 May 2023
Revised date: 7 August 2023
Accepted date: 28 August 2023

Please cite this article as: Alexander Misol, Ilenia Giarnieri, Francesca Ospitali, Adriana Ballarini, José Jiménez-Jiménez, Enrique Rodríguez-Castellón, Francisco Martín Labajos, Giuseppe Fornasari and Patricia Benito, CO_2 hydrogenation over Ru hydrotalcite-derived catalysts, *Catalysis Today,* (2023) doi:https://doi.org/10.1016/j.cattod.2023.114362

CO_2 hydrogenation over Ru hydrotalcite-derived catalysts

Alexander Misol,[1,2] Ilenia Giarnieri,[1,3] Francesca Ospitali,[1] Adriana Ballarini,[4] José Jiménez-Jiménez,[5] Enrique Rodríguez-Castellón,[5] Francisco Martín Labajos,[2] Giuseppe Fornasari,[1,3] Patricia Benito[1,3,*]

[1]Dipartimento Chimica Industriale "Toso Montanari", Università di Bologna, Viale Risorgimento 4, 40136, Bologna, Italy.

[2]GIR-QUESCAT. Departamento de Química Inorgánica. Universidad de Salamanca, Plaza de los Caidos s/n, 37008, Salamanca, Spain

[3]Center for Chemical Catalysis – C3, Alma Mater Studiorum – Università di Bologna, Viale Risorgimento 4, 40136, Bologna, Italy

[4]Instituto de Investigaciones en Catálisis y Petroquímica "Ingeniero José M. Parera", Facultad de Ingeniería Química, Universidad Nacional del Litoral-CONICET, Colectora Ruta Nacional N° 168 km. 0, Pje. El Pozo, Santa Fe, Argentina

[5]Universidad de Málaga, Departamento de Química Inorgánica, Facultad de Ciencias. 29071 Málaga, Spain.

*patricia.benito3@unibo.it

Abstract

The hydrogenation of CO_2 over Ru catalysts is structure sensitive, the selectivity of the process can be driven either to the production of CH_4 or CO depending on Ru particles and support features. Herein, Ru-based MgAl-HT (HT=hydrotalcite) derived catalysts with different Ru loadings (0.5, 1, and 2 wt.%) and promoted with La^{3+} were prepared, characterized, and tested for CO_2 methanation at high Gas Hourly Space Velocity values (480 L / g_{cat} h) feeding a $CO_2/H_2/N_2$ = 1/4/1 v/v mixture. The $MgAlO_x$ mixed oxide obtained after calcination at 600 °C and reduction provided weak, medium and mainly strong basic sites, able to activate the CO_2 molecule, and hosted very small Ru

nanoparticles (1-3 nm). However, the catalysts displayed a low activity in the low temperature range and a poor selectivity to CH_4. The addition of La^{3+}, despite contributing to the basicity, did not have any significant effect on performance. In a comparison between Ru- and Ni-HT-derived catalysts, tested under similar reaction conditions, Ni largely overperformed Ru.

Keywords: hydrotalcite, Ruthenium, CO_2, CH_4, CO.

1. Introduction

Concern for environmental and resource protection, along with the growing energy demand, has prompted the development of catalytic technologies to convert greenhouse gases into value-added products. This concept is at the heart of so-called C1 chemistry, which uses compounds containing a single carbon atom such as CO_2 and CH_4 to produce value-added compounds or fuels [1].

The valorization of CO_2 through hydrogenation to CH_4 (methanation or Sabatier reaction) has been widely investigated in the last decade to develop enhanced catalysts and handle the heat generated by this exothermic reaction [2-6]. Ni-based catalysts are usually the best choice [7,8]. They are inexpensive and their activity in the low temperature range, initially poorer than for Ru catalysts [9-12], has been enhanced by tailoring the type of support and promoters. However, Ni is prone to deactivation by sulfur, water, and oxygen; consequently, catalysts could significantly decrease their activity in the conversion of real CO_2 streams, e.g. flue gases, and in adsorption/methanation cycles [13]; for these applications, Ru-catalysts are considered more suitable [14-17].

The performance of Ru-based catalysts in CO_2 hydrogenation is structure sensitive [18-21] and therefore depends on the Ru loading [20,22-28]. The selectivity of the process over these catalysts can vary from 100 % towards CH_4 to 100 % towards CO [29]. It is widely agreed that when using Al_2O_3 as a support, Ru loadings between 2.5 and 5 wt.% are required to drive the process towards the production of CH_4, due to the formation of Ru nanoparticles in the 5-10 nm range either after reduction or during the reaction [19,23,26,28]. The key role of a high Ru loading and large agglomerates or clusters in achieving a high CH_4 selectivity is confirmed for other non-reducible

supports, e.g., MgO, $MgAl_2O_4$ [30] and also for reducible TiO_2 [20]. However, some deviations to this Ru particle size-selectivity tradeoff are reported when Ru is deposited on modified Al_2O_3 (i.e., containing highly basic hydroxylated alumina sites [24] or alkali doped [31]), high surface area MgO [25] or reducible supports (e.g. CeO_2 [32-34], TiO_2 [35,36] and ZrO_2 [37]) due to the role of the support on the CO_2 activation, Ru electronic modification or O mobility. For instance, on a high surface area MgO support, which also provides sites for CO_2 activation, small nanoparticles (2-4 nm) display good activity [25]. Furthermore, small nanoparticles or even single atoms reached full CH_4 selectivity in combination with CeO_2 [32].

Bulk Ni catalysts derived from hydrotalcite-type (HT) compounds show advantages in comparison to supported catalysts in CO_2 methanation [38-40]. Calcination of a NiMgAl hydrotalcite-type structure at moderate temperatures (e.g. 600 °C) followed by reduction generates a catalyst that combines the basic sites of a $MgAlO_x$ mixed oxide with highly dispersed Ni nanoparticles [41]. The properties of the catalysts are enhanced by the addition of rare-earth elements such as La^{3+} [40,42]. Despite the well-known superior properties of HT-derived Ni catalysts for CO_2 methanation, to the best of our knowledge, the application of Ru-based HT-derived catalysts for this reaction is scarce [43], although Ru^{3+} can be inserted in the lamellar structure of the HT and consequently generate highly dispersed Ru nanoparticles [44] and in turn catalysts for the conversion of real CO_2 streams, and in adsorption/methanation cycles. Non-thermal plasma activated CO_2 hydrogenation was performed over Ru/MgAl catalysts prepared by impregnating Ru on MgAl HTs and directly reducing this material [43]; plasma-catalyst interactions enable alternative pathways for promoting CO_2 hydrogenation than the conventional thermocatalytic process. Moreover, Ru was impregnated on a $NiMgAlO_x$ HT-derived material to prepare a Ru-Ni bimetallic catalyst [45].

In this work, Ru-based catalysts obtained from coprecipitated RuMgAl HT compounds were studied in the hydrogenation of pure CO_2 at high Gas Hourly Space velocity (GHSV) values (480 L/g_{cat} h, similar to those previously used by us for Ni HT-derived catalysts [40,41]), as a first step in

the development of these catalysts, which potential applications for the conversion of real CO_2 streams. First, the effect of Ru loading (0.5, 1.0, and 2.0 wt.%) on CO_2 conversion and CH_4/CO selectivity was investigated. Then La^{3+} was added to the 1 wt.% Ru catalyst to modify the support basicity. The catalysts, as prepared and after catalytic tests, were characterized to correlate the performance with the physicochemical properties. For comparison purposes, a 1wt.% Ru/Al_2O_3 catalyst was prepared by incipient wetness impregnation, characterized and tested in the reaction.

2. Experimental section

2.1. Preparation of the catalysts

The catalysts were prepared by the co-precipitation method at constant pH [41]. First, 1.0 M cation solutions of Ru/Mg/Al were prepared molar ratios 0.22/70/29.78, 0.44/70/29.56 and 0.9/70/29.1 to obtain a wt.% Ru in the final catalyst of 0.5, 1 and 2 wt.%, respectively. Similarly, the cation solution of Ru/La/Mg/Al was prepared in a molar ratio of 0.5/5/70/24.5 to obtain a 1 wt.% Ru in the final catalyst. Mg^{2+}, La^{3+} and Al^{3+} cations were added to the solution as nitrates ($Mg(NO_3)_2{\cdot}6H_2O$, $Al(NO_3)_3{\cdot}9H_2O$, $La(NO_3)_3{\cdot}6H_2O$) and the Ru^{3+} cation as chloride salt ($RuCl_3{\cdot}3H_2O$). The precipitation of the catalyst precursors was carried out into a batch reactor containing a 2.0 M Na_2CO_3 solution at 60 °C under stirring, where the cation solutions were dropped. The pH was kept constant at 10.0 ± 0.1 by adding the necessary volume of a 3 M NaOH solution. A suspension was obtained and left to age while being subjected to intense magnetic stirring for 1 h at 60 ºC. Finally, the slurry was filtered and washed thoroughly with ultrapure water until pH 7.0 to remove the counterions of the starting salts (nitrate, chloride and sodium). The filtration cake was dried overnight in an oven at 40 °C and then ground to obtain a fine powder of HT catalyst precursors. The precursors were subsequently calcined at 600 °C for 6 h with a heating ramp of 10 °C/min. The catalysts were named as RuMgAl or RuLaMgAl followed by the Ru wt.%, for example, RuMgAl-1%.

A Ru/Al_2O_3 catalyst was prepared by incipient wetness impregnation (IWI) to obtain a 1 wt.% Ru loading. A 0.015 w/v Ru solution was prepared from the $Ru(NO)(NO_3)_3$ salt. The solution was

dropped over 1 g of γ- Al_2O_3 (195 m^2/g) grounded into a fine powder. The slurry was dried in air oven at 40 °C and then it was calcined at 600 °C for 6 h with a heating ramp of 10 °C/min.

The catalytic tests were carried out after pelletization of the calcined solid using a SPECAC laboratory hydraulic press. The pellet was manually ground in a mortar and sieved to select the solid fraction with a particle size of 0.420 - 0.595 mm (sieve mesh 40-30), a size suitable for further dispersion in the quartz bed of equal particle size.

2.2. Characterization techniques

Powder X-ray diffraction (XRD) patterns were recorded in a PANalytical X'Pert diffractometer. The diffractometer was equipped with a Cu-Kα radiation (λ_{mean} = 0.15418 nm) and a fast X'Celerator detector. Wide-angle diffractogram was collected over 2θ range from 5 to 80° with a step size of 0.05° and scan time 15.25 s per step.

Specific surface areas of the catalysts were assessed from N_2 (L'Air Liquide, 99.999%) adsorption-desorption isotherms at -196 °C, recorded in a Micromeritics ASAP 2020 instrument. Prior to measurements, 0.15 g powder catalysts samples were degassed under vacuum (< 30 μm Hg) at 150 °C for HT precursors (or at 250 °C for calcined catalysts) and maintained for 30 min before performing the measurement. The specific surface area (S_{BET}) was calculated using the Brunauer-Emmett-Teller (BET) multiple-point method in the relative pressure range P/P_0 from 0.05 to 0.3.

Hydrogen temperature programmed reduction (H_2-TPR) was performed on an AutoChem II (Chemisorption analyzer, Micromeritics). An amount of 100 mg of pelletized catalyst was first pretreated at 150 °C with a He flow of 30 mL/min for 30 min. After cooling to 40 °C in a He atmosphere, the carrier gas was switched to 5 % H_2/Ar (v/v) at 30 mL/min. Once the baseline was stabilized, the temperature was raised to 900 °C with a 10 °C/min ramp. The outlet stream passed through an ice trap to condense the water vapor generated during the reduction. The H_2 flow rate was measured using a thermal conductivity detector (TCD).

The basicity of the samples was determined by thermo-programmed desorption of CO_2 (TPD-CO_2) using an AutoChem 2920 apparatus. Prior to each analysis, approximately 100 mg of pellet sample was heated at 150 °C for 30 min in He (50 mL/min) and then cooled to 40 °C. The catalyst was then reduced at 600 ºC (5 °C/min heating rate) for 2 h under 5% H_2/Ar (v/v) (50 mL/min). After that, CO_2 was adsorbed by introducing a 50 mL/min flow of pure CO_2 at 40 °C for 15 min. The sample was then flushed with 50 mL/min He for 60 min to remove weakly adsorbed CO_2. CO_2-TPD measurements were performed by increasing the temperature from 40 to 600 °C with a heating rate of 30 °C/min. The desorption of CO_2 was monitored with a TCD and using a mass spectrometer Cirrus 2. In this work, the evolution of the intensity of the signal at m/z = 44 was reported. The desorption profile was deconvoluted using Origin 8.0 software.

High resolution transmission electron microscopy (HRTEM) characterization was performed using TEM/STEM FEI TECNAI F20 microscope, equipped with an EDS (Energy-dispersive X-ray spectroscopy) analyzer. The finely powdered catalyst was suspended in ethanol under the action of ultrasounds for 20 min. The suspension was then applied to a Cu grid with holey quanti-foil carbon film, which was dried at 100 °C before the measurement. STEM/HAADF (Scanning Transmission Electron Microscope/High-angle annular dark-field) images were recorded to calculate the particle size distributions. Particle size distributions were processed with approximately 200 particles in three different zones for each sample.

The surface of the samples was studied by X-ray Photoelectron Spectroscopy (XPS) by using a Physical Electronics VersaProbe II Scanning XPS Microprobe spectrometer equipped with monochromatic X-ray Al Kα radiation. The binding energies were referenced to the C 1*s* peak from adventitious carbon at 284.5 eV. High-resolution spectra were recorded in a 29.35 eV constant energy pass, using a 200 µm diameter analysis area, and the pressure in the analysis chamber was kept below 5×10^{-6} Pa. PHI ACCESS ESCA-F V6 software was used for data acquisition and analysis. The

recorded spectra were analyzed with Gauss-Lorentz curves to determine more accurately the binding energy of the atomic levels of the different elements.

2.3. Catalytic tests

The catalytic tests were performed in a fixed-bed quartz reactor, with a diameter of 10.0 mm, placed in an electrically heated furnace, at 1 bar. The catalytic bed, consisting of the catalyst in pellet form (30 mg) dispersed in 470 mg of quartz with the same particle size (0.420 – 0.595 mm), was placed in the reactor. The height and volume of the catalytic bed were 5 mm and 377 mm^3, respectively. The catalytic bed was placed on a bed of quartz wool seated on an α-Al_2O_3 monolith. The furnace temperature was kept constant whereas the catalyst temperature changed depending on the exothermic nature of the reaction. The gas temperature was measured with a K-type thermocouple (0.5 mm diameter) sliding in a 2 mm quartz sheath inside the catalyst bed. The temperature was measured along the catalytic bed according to a previous work [40].

The catalyst activation was carried out by *in situ* reduction at 600 ºC with a flow of 200 mL/min of H_2/N_2 = 1/1 (v/v) for 2 h, with a heating ramp of 10 ºC/min. After cooling to 200 °C and maintaining this temperature for 30 min, the reaction gas ($CO_2/H_2/N_2$ = 1/4/1 v/v) was injected with a total flow rate of 240 mL/min, corresponding to a GHSV (Gas Hourly Space Velocity) of 480 L/g_{cat} h. The high GHSV has two main purposes: i) to better highlight the differences in activity at low temperature moving away from thermodynamic equilibrium; ii) decrease the size of the reactor, whenever heat removal is possible. The catalytic tests were carried out in reaction cycles between 200 and 600 °C (only the results above 275 °C are shown since they catalysts were inactive below this value), the temperature being increased at 25 °C intervals up to 450 °C and at 50 °C between 450 and 600 °C. After passing through a cold trap for water condensation, the outlet stream was analyzed online by an Agilent 990 microGC, equipped with two thermal conductivity detectors (TCD) and a Molecular Sieve 5A SS column using Ar as a carrier for H_2, CO and CH_4 analysis and a PoraPLOT

U using He as carrier for CO_2 quantification. Since no C_{2+} hydrocarbons were detected, CO_2 conversion, CH_4 and CO selectivities were defined as follows:

$$CO_2 \text{ conversion } (\%) = \frac{[CH_4]+[CO]}{[CH_4]+[CO]+[CO_2]} x100 \quad (1)$$

$$CO \text{ selectivity } (\%) = \frac{[CO]}{[CH_4]+[CO]} x100 \quad (2)$$

$$CH_4 \text{ selectivity } (\%) = \frac{[CH_4]}{[CH_4]+[CO]} x100 \quad (3)$$

where [A] (A = $[CH_4]$, [CO], and $[CO_2]$) stands for the molar ratio of component A in the outlet stream.

3. Results and discussion

3.1. Effect of the Ru loading

The diffraction patterns of the precipitated samples in Figure S1 confirmed the formation of the hydrotalcite-like structure for all three Ru loadings [46]. After calcination at 600 °C (Figure 1a), the characteristic $MgAlO_x$ mixed oxides derived from HT-compounds were obtained, namely, a MgO rock-salt structure where Al^{3+} ions were inserted. The reflections of a segregated RuO_2 rutile-type crystalline phase were only observed for the high loaded RuMgAl-2% catalyst. Conversely, for the Ru/Al_2O_3 catalyst, the RuO_2 reflections were intense (Figure S2a). All the catalysts derived from HT compounds display specific surface area values around 190 m^2/g (196-182 m^2/g) (Table S1), similar to the value of the impregnated Ru/Al_2O_3 sample (185 m^2/g). The impregnation of the Al_2O_3 with Ru and the following calcination did not significantly modify the specific surface area of the original support (195 m^2/g).

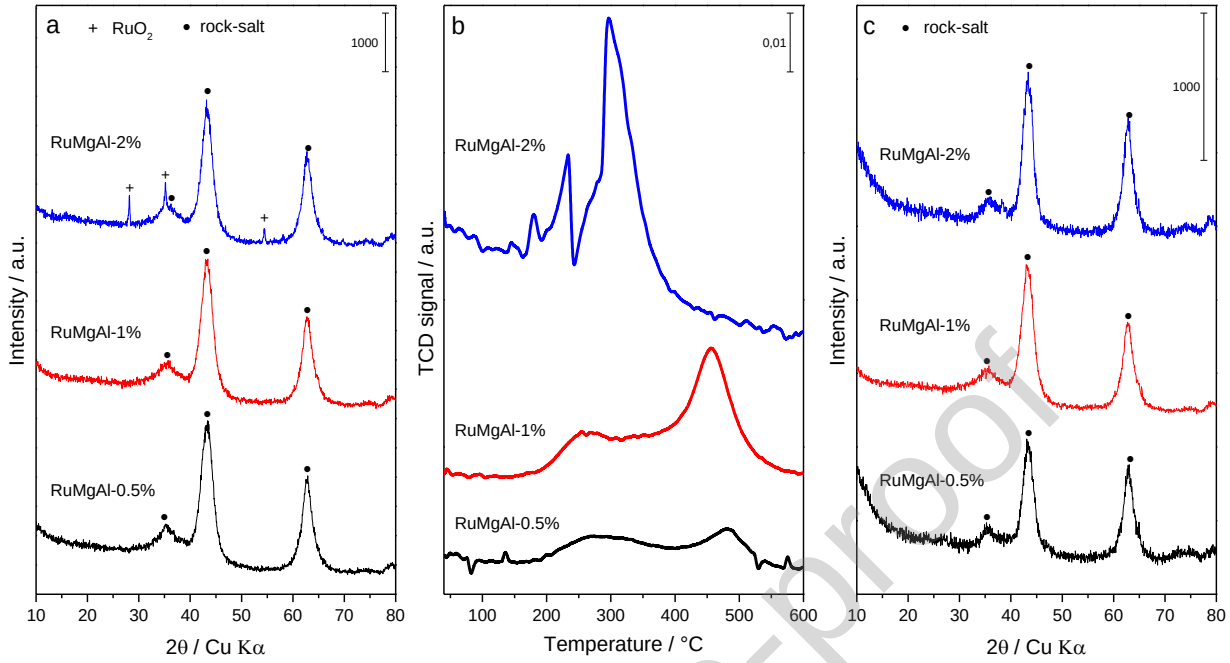

Figure 1. Diffraction patterns (a) and H_2-TPR profiles (b) of HT-derived catalysts with different Ru loadings; (c) Diffraction patterns of catalysts after tests in the hydrogenation of CO_2.

The effect of Ru loading on the reducibility of HT-derived catalysts was investigated by H_2-TPR (Figure 1b). The profiles showed H_2 consumption peaks at around 250 and 450-475 °C in the low loaded catalysts, the latter being more intense for RuMgAl-1%. The low temperature peak was related to the reduction of well-dispersed RuO_x and bulk RuO_2 species [44,47]. Meanwhile, the high reduction temperature indicated the presence of ruthenium species highly interacting with the oxidic matrix [44,48]. These results suggested that the absence of RuO_2 reflections in the diffraction patterns of low loaded 1 and 0.5 wt.% Ru catalysts was likely attributed to its high dispersion in the oxidic matrix. Indeed, the high reduction temperature peak disappeared in the high loaded RuMgAl-2% catalyst, where Ru segregated as RuO_2 was clearly identified in the diffraction pattern; in this catalyst the second peak moved to ca. 300 °C, suggesting a lower interaction between the ruthenium species and the support or the presence of higher particles. The reduction profile of the impregnated Ru/Al_2O_3 catalyst showed two overlapped H_2 consumptions in the 200-300 °C interval (Figure S2b), related to

well dispersed RuO_x and RuO_2 particles [49], interacting more weakly with the support than for HT-derived catalysts.

The high-resolution Ru $2p_{3/2}$ core level spectrum of RuMgAl-1% confirmed the presence of Ru^{4+}, signal at 464.7 eV, which coexisted with Ru^0 (462.0 eV) (Table 1 and Figure S3). The formation of Ru^0 could occur during the calcination process. The Ru^{4+} and Ru^0 percentages were 56 and 44 %, respectively [50,51]. The concentration of Ru species on the surface was around 2 wt.%, higher than the one in the bulk. Meanwhile, the Mg/Al ratio was 2.0, in line with the 2.1 theoretical value. The high-resolution Ru $2p_{3/2}$ spectrum of the impregnated Ru/Al_2O_3 catalyst also evidenced the presence of both Ru^{4+} and Ru^0 species, the latter one being more abundant (75 %). The BE of the Ru^{4+} species on the Al_2O_3 support was shifted towards slightly higher energies (465.5 eV), probably due to a different interaction active phase-support [51,52]. More remarkably, the concentration of the Ru species on the surface of the Al_2O_3 support largely overcome the theoretical one.

Table 1. Identification of Ru species on the surface, Ru content and Mg/Al atomic surface ratio

Catalyst	**Ru $2p_{3/2}$ BE / eV**	**Ru wt.%**	**Mg/Al ratio**
RuMgAl-1% fresh	462.0 (44) 464.7 (66)	1.93	2.0
RuMgAl-1% reduced	462.9 (100)	1.54	2.0
Ru/Al_2O_3 fresh	462.3 (75) 465.5 (25)	4.95	-
Ru/Al_2O_3 reduced	461.7 (80) 465.6 (20)	0.90	-

The numbers in brackets referred to the % of the species.

The basicity of RuMgAl-1%, as a representative of the HT-derived catalysts, was evaluated by CO_2-TPD (Figure 2); the low Ru loadings in the catalysts did not modify the basic properties of the materials. The measurement was performed over the catalyst *in situ* reduced at 600 °C to try to

mimic the state of the catalyst under reaction conditions. A broad CO_2 removal peak was recorded in the 100 °C to 550 °C temperature range. Deconvolution of the signal into three peaks centered at 140, 200, and 320 °C, (Figure S4) indicated the presence of weak (OH), medium (acid-base Lewis pairs), and strong basic sites (O^{2-}), which adsorb hydrogen carbonate, bidentate carbonates and monodentate carbonate species respectively [53]. The CO_2 total uptake was 0.450 mmol/g_{cat}, the strong basic sites were the most abundant (66 %), followed by medium (22 %), and weak ones (13 %). It should be noted that medium basic sites were reported to be the most active for the methanation process [54].

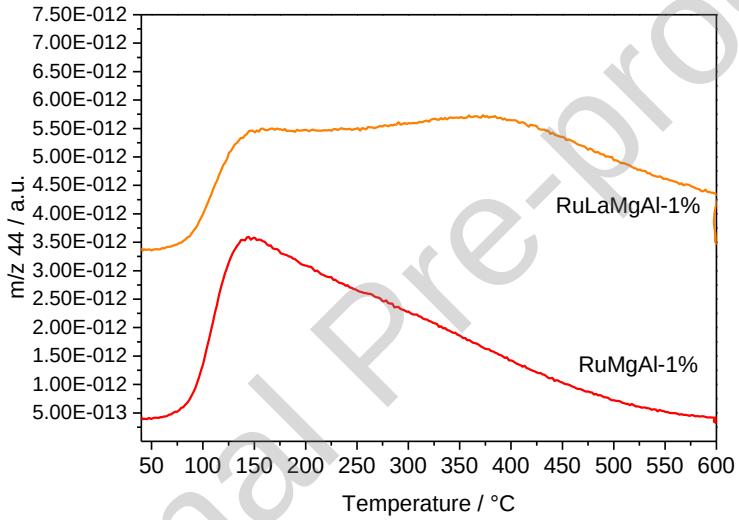

Figure 2. CO_2-TPD profiles of RuMgAl-1% and RuLaMgAl-1% catalysts reduced at 600 °C.

The values of CO_2 conversion and selectivity to CO and CH_4 obtained on the three HT-derived catalysts are displayed in Figure 3. All three catalysts were inactive at oven temperatures below 325 °C (Figure 3a). After the reaction light-off, the conversion increased steadily up to 600 °C. Ru loading only had a minor effect on conversion when shifting from 0.5 wt.% to 1 wt.%. Remarkably, CO_2 conversion curves were similar for RuMgAl-1% and RuMgAl-2%. This behavior deviated from the commonly observed improvement in performance by increasing the Ru loading from 1 to 2 wt.% [19,21]. More surprisingly, CH_4 selectivity was very low, i.e., CO was the main reaction product. The CH_4 formation increased both with Ru loading and reaction temperature (Figure 3b). For instance, over the low loaded RuMgAl-0.5 % catalyst at 350 °C, the selectivity to CH_4 was around 20 %

(selectivity to CO ca. 80 %) and slightly increased until reaching ca. 29 % at 550 °C. Conversely, the production of CO was more suppressed over RuMgAl-2% as the temperature raised, similar selectivity values to CO (50 %) and CH_4 (50 %) were obtained at 500 and 550 °C. Temperature profiles were recorded along the axial direction in the center of the catalytic bed (Figure S5). The temperature was constant along the catalytic bed under all reaction conditions in agreement with a low contribution from the exothermic methanation reaction.

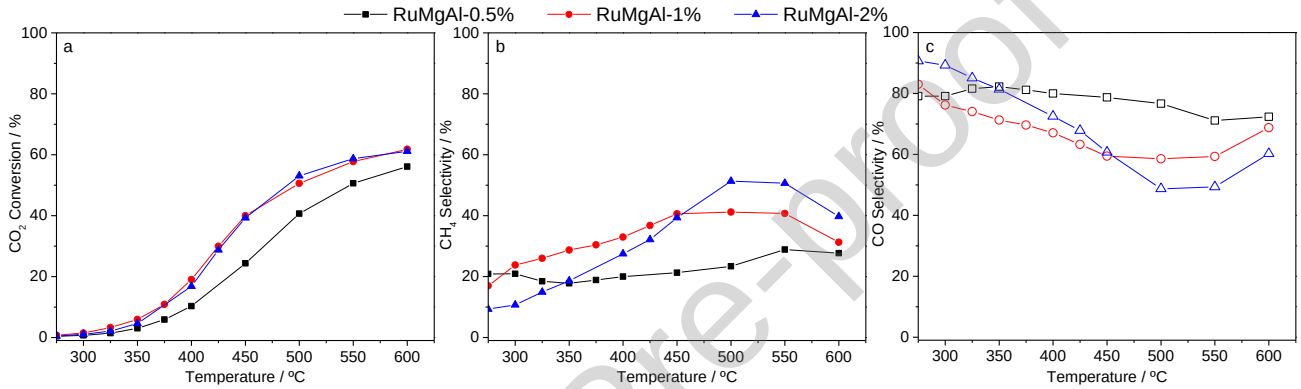

Figure 3. Effect of the Ru loading in RuMgAl HT-derived catalysts on the CO_2 conversion (a), CH_4 selectivity (b), and CO selectivity (c).

The catalytic results followed an anomalous trend, with a good Ni methanation catalyst, under the same reaction conditions, the CO selectivity increased with temperature due to the contribution of the reverse water gas shift (RWGS) [41]. In this work, we only observed a drop in the CH_4 selectivity at 600 °C oven temperature. A reconstruction/sintering of the catalyst that activates the catalyst due to the growth of the Ru particle size or modification of the support as previously reported for Ru/Al_2O_3 [19,28,55] could explain the catalytic results. To check the stability of the catalysts, tests were carried out at the end of the first cycle over RuMgAl-1%. The activity and the selectivity of the catalyst in the second reaction cycle were similar to the values in the first run (Figure S6). Hence, the increase in CH_4 selectivity with temperature could not be related to the sintering of Ru particles. The diffraction patterns of all three catalysts after the catalytic tests evidenced the stability of the $MgAlO_x$ support, since the patterns before and after reaction were similar, with the exception

of the disappearance of the RuO_2 phase due to the catalyst reduction (Figure 1c). Moreover, the absence of reflections due to the Ru^0 phase suggested the formation of small nanoparticles.

Considering that the reaction took place through the formation of Ru-CO intermediates [20], it could be hypothesized that Ru species were saturated by CO and therefore there were not enough sites to activate the H_2 molecule, and consequently formation of CO selectivity instead of CH_4 was preferred. This behavior likely depended on the GHSV, which in this work was very high (480 L/g_{cat} h). However, the tests carried out on the impregnated Ru/Al_2O_3 catalyst under the same reaction conditions showed that the production of CH_4 was favored over the production of CO and it followed the expected trend, i.e., it decreased as the reaction temperature did (Figure 4).

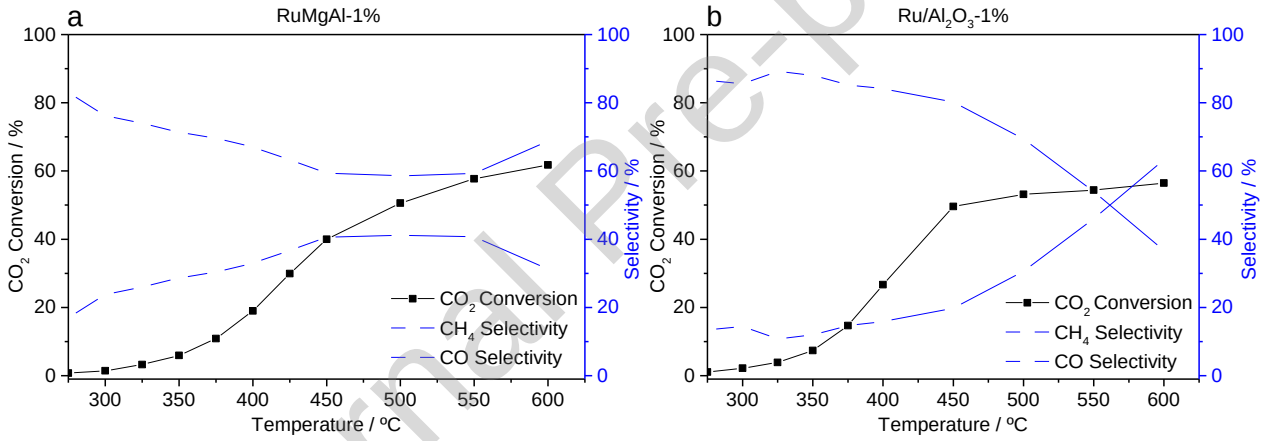

Figure 4. Comparison of the catalytic activity in the CO_2 hydrogenation of the RuMgAl HT-derived (a) and Ru/Al_2O_3 (b) catalysts.

To explain the differences in the catalytic activity of the RuMgAl-1% HT-derived and Ru/Al_2O_3, the reduced and spent catalysts were characterized. The high-resolution Ru $2p_{3/2}$ core level spectra of RuMgAl-1% and Ru/Al_2O_3 reduced at 600 °C revealed that in both types of catalysts ruthenium species were in the metallic state (Table 1). Their concentration on the catalyst surface decreased during reduction, likely due to agglomeration in larger Ru particles, and it was slightly higher on the HT-derived than on the Al_2O_3 supported catalyst (1.5 vs 0.90 %). Considering that both catalysts had similar specific surface areas (ca. 190 m^2/g), the concentration of Ru on the catalyst surface of the freshly reduced catalysts could not explain the differences in the selectivity of the

process. This also suggested that the embedment of Ru in the bulk of HT-derived catalysts was not responsible for the low activity. STEM/HAADF images showed that the RuMgAl-1% catalyst contained Ru nanoparticles (NPs) with a narrow particle size distribution from 0.5 to 3 nm (Figure 5a), similar to those obtained in a high surface area MgO [25]. Conversely, in the 1 wt.% Ru/Al_2O_3 catalyst a broad distribution of larger Ru NPs (from 2 to 25 nm) was obtained (Figure 5b). These larger Ru NPs were responsible for the Ru^0 reflections clearly identified in the diffraction pattern of the Ru/Al_2O_3 (Figure S2a), while the very small NPs in the HT-derived catalyst could not be detected by XRD (Figure 1c). The formation of small Ru NPs (1-3 nm) was also demonstrated for the RuMgAl-2% spent catalyst (Figure S7a), though in this case also large particles were identified (Figure S7b). However, under our reaction conditions in this work, a moderate dispersion of Ru particles, as in the impregnated Ru/Al_2O_3 catalyst, was preferred to achieve a higher selectivity in CH_4, likely related to a lower Ru-CO interaction and coverage [32,56] or to a stronger H-spillover effect [32] from large Ru NPs.

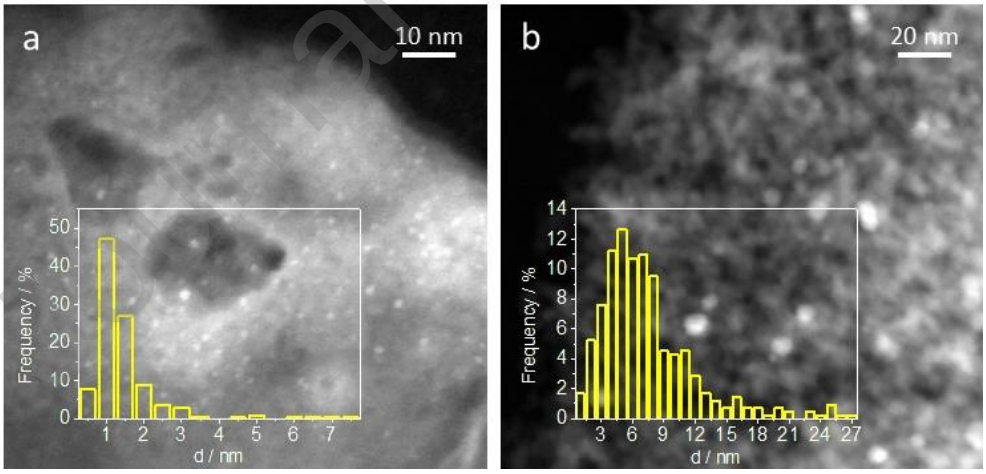

Figure 5. STEM/HAADF images and Ru particle size distribution in RuMgAl-1% (a) and Ru/Al_2O_3 (b) catalysts. The brighter dots correspond to the Ru particles.

3.2. Effect of the basicity. La^{3+} incorporation

The well-known basic properties of the Ru HT-derived catalyst were also confirmed in this work; however, the combination of small Ru NPs with a basic support did not provide active sites suitable

for the selective hydrogenation of CO_2 to CH_4 as previously reported for Ru on MgO [25]. This behavior could be related to the presence of strong basic sites (less active than medium basic sites [54]) and/or to a low H-spill over from Ru to the CO_2 species activated on the support surface or at the Ru-support interface. Since the increase in the Ru loading from 1 to 2 wt.% did not significantly modify the Ru particle size or the H-spill over process, an attempt was made to improve the activity through the modification of the basicity of the $MgAlO_x$ matrix. A catalyst was prepared incorporating La^{3+} cations (RuLaMgAl) [40,41,57].

The large ionic radius and strong anionic character of La^{3+} provoked that part of the cations was outside the brucite-type layers as $LaCO_3OH$ and $La_2(CO_3)_2(OH)_2$ side phases (Figure S8) [41]. Accordingly, after calcination at 600 °C, $La_2O_2CO_3$ was also observed in the catalyst (Figure 6a). The presence of La^{3+} did not modify the reducibility of the catalyst (Figure 6b); H_2 consumption was related to well dispersed RuO_x and Ru^{4+} species that highly interacted with the oxidic matrix. As expected, La^{3+} provoked an increase in the CO_2 uptake; however, it was mainly due to the development of additional strong basic sites (cf. the more intense CO_2-TPD signal at ca. 320 °C in Figure 2). Unfortunately, the signal in the TPD profile did not return to the baseline at the end of the measurement (600 °C), which made it not possible to perform the peak deconvolution and to an underestimation the total CO_2 uptake.

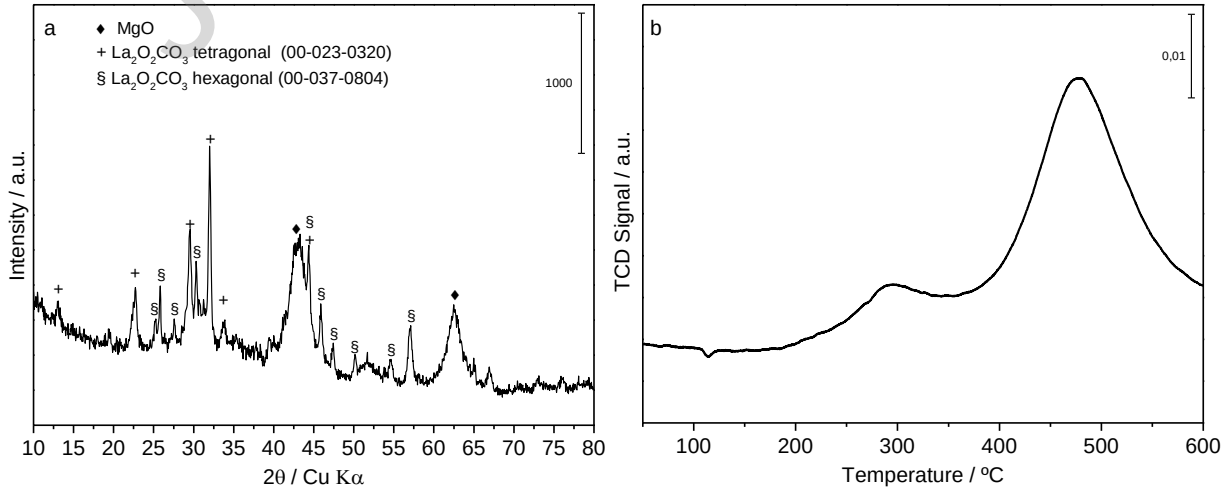

Figure 6. Diffraction pattern (a) and H_2-TPR (b) profile of the RuLaMgAl catalyst.

Regrettably, the modification of the basicity of the oxidic matrix did not have any positive effect, as previously observed for Ni HT-derived catalysts (Figure 7). The CO_2 conversion roughly followed the same trend as in the RuMgAl-1% catalyst (Figure 7a). Contrarily, CH_4 production was further suppressed; the selectivity to CH_4 decreased (and therefore the selectivity to CO increased) ca. 10-12 % (Figure 7b).

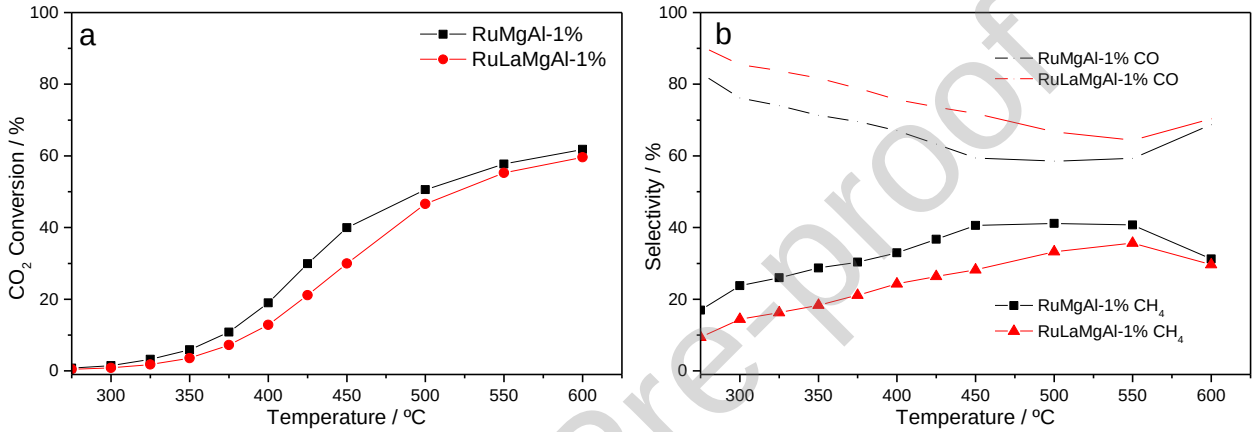

Figure 7. Effect of the addition of La to the catalyst formulation on the CO_2 conversion (a) and selectivity to CH_4 and CO (b).

The catalytic data and the characterization results showed that though CO_2 could be activated on both the HT-derived support and the Ru particles, the activity was limited to the production of CO, likely due to the Ru^0 small particle size and the poor H_2 activation [19]. CO_2 may firstly interact with the support, but then it was not hydrogenated to CH_4, and it was only reduced to CO. Some unreactive CO species were reported by Wang et al. and identified as geminal CO molecules adsorbed on low-coordinated sites [23]. A Langmuir–Hinshelwood type mechanism was proposed wherein the H-assisted dissociation of the reactive CO was the rate-determining. Similarly, the quasi-saturation of Ru particles with CO and the limitation of the reaction by the competitive Langmuir-type co-adsorption of H_2 was reported by Dreyer et al. [56]. A higher reaction temperature could weaken the Ru-CO bond and promote the H-spill over, therefore the CO_2 conversion to CH_4 could increase,

explaining the enhancement in the CH_4 selectivity observed during the catalytic cycle in Figures 3 and 7.

Comparing the performance of the Ru-HT derived catalysts with the performance of Ni-HT derived catalysts previously reported by us [40,41], tested under the same reaction conditions, it was clear that the latter largely outperform the Ru-based catalysts. For instance, a Ni50Mg25La5Al20 catalyst at 250 °C oven temperature reached a CO_2 conversion close to 60 % and almost full CH_4 selectivity (98 %) [41], while the Ru catalysts were inactive. The higher activity of Ni in comparison to Ru agrees with previously results obtained in a 1 kW reactor [58], where the activity of Ni-based catalyst was about 3 times higher than the activity of the Ru-based catalyst at 275 °C.

4. Conclusions

Ru-containing MgAl hydrotalcite-type compounds as precursors of catalysts for CO_2 hydrogenation allowed the formation of small (1-3 nm) Ru nanoparticles strongly interacting with the basic $MgAlO_x$ matrix. However, the combination of these important features for CO_2 methanation did not provide active and selective catalytic sites for the selective conversion of CO_2 to CH_4. The catalysts were poorly active, requiring temperatures above 300 °C to initiate the CO_2 conversion, and they drove the reaction mainly to CO production, even after tailoring the basicity by adding of La^{3+}. Comparison with a more CH_4-selective Ru/Al_2O_3 catalyst suggested that the small Ru NPs were responsible of the poor ability of the catalysts to produce CH_4 and that the basic properties of the support played only a marginal role when the ability of the catalyst to adsorb CO and to activate H_2 was not optimized. To develop HT-derived Ru catalysts for the selective production of CH_4 further work is required to optimize the Ru particle size, as well as to better characterize the Ru-CO interaction and the H_2 activation in situ or operando.

Acknowledgements

J.J.J., P.B. and E.R.C. thank to Spanish Ministry of Science and Innovation, project PID2021-126235OB-C32 funded by MCIN/ AEI/10.13039/501100011033/ and FEDER funds, and project TED2021-130756B-C31 funded by MCIN/AEI/10.13039/501100011033 and by "ERDF A way of making Europe" by the European Union NextGenerationEU/PRTR. A.M. thanks Junta de Castilla y León and the European Social Fund for a PhD contract and to the University of Salamanca for the aid to carry out the research stay.

References

[1] Y. Liu, D. Deng, X. Bao, Catalysis for Selected C1 Chemistry, Chem. 6 (2020) 2497–2514. doi:10.1016/j.chempr.2020.08.026.

[2] S. Rönsch, J. Schneider, S. Matthischke, M. Schlüter, M. Götz, J. Lefebvre, P. Prabhakaran, S. Bajohr, Review on methanation – From fundamentals to current projects, Fuel. 166 (2016) 276–296. doi:10.1016/j.fuel.2015.10.111.

[3] M. Thema, F. Bauer, M. Sterner, Power-to-Gas: Electrolysis and methanation status review, Renew. Sustain. Energy Rev. 112 (2019) 775–787. doi:10.1016/j.rser.2019.06.030.

[4] J. Ashok, S. Pati, P. Hongmanorom, Z. Tianxi, C. Junmei, S. Kawi, A review of recent catalyst advances in CO_2 methanation processes, Catal. Today. 356 (2020) 471–489. doi:10.1016/j.cattod.2020.07.023.

[5] C. Wulf, P. Zapp, A. Schreiber, Review of Power-to-X Demonstration Projects in Europe, Front. Energy Res. 8 (2020) 1–12. doi:10.3389/fenrg.2020.00191.

[6] W.J. Lee, C. Li, H. Prajitno, J. Yoo, J. Patel, Y. Yang, S. Lim, Recent trend in thermal catalytic low temperature CO_2 methanation: A critical review, Catal. Today. 368 (2021) 2–19. doi:10.1016/j.cattod.2020.02.017.

[7] H. Muroyama, Y. Tsuda, T. Asakoshi, H. Masitah, T. Okanishi, T. Matsui, K. Eguchi, Carbon dioxide methanation over Ni catalysts supported on various metal oxides, J. Catal. 343 (2016) 178–184. doi:10.1016/j.jcat.2016.07.018.

[8] P. Strucks, L. Failing, S. Kaluza, A Short Review on Ni-Catalyzed Methanation of CO_2: Reaction Mechanism, Catalyst Deactivation, Dynamic Operation, Chemie Ing. Tech. 93 (2021) 1526–1536. doi:10.1002/cite.202100049.

[9] M. Nurunnabi, K. Fujimoto, K. Suzuki, B. Li, S. Kado, K. Kunimori, K. Tomishige, Promoting effect of noble metals addition on activity and resistance to carbon deposition in oxidative steam reforming of methane over NiO–MgO solid solution, Catal. Commun. 7 (2006) 73–78. doi:10.1016/j.catcom.2005.09.002.

[10] W. Wang, S. Wang, X. Ma, J. Gong, Recent advances in catalytic hydrogenation of carbon dioxide, Chem. Soc. Rev. 40 (2011) 3703. doi:10.1039/c1cs15008a.

[11] C. Vogt, M. Monai, G.J. Kramer, B.M. Weckhuysen, The renaissance of the Sabatier reaction and its applications on Earth and in space, Nat. Catal. 2 (2019) 188–197. doi:10.1038/s41929-019-0244-4.

[12] E. Moioli, A. Züttel, A model-based comparison of Ru and Ni catalysts for the Sabatier reaction, Sustain. Energy Fuels. 4 (2020) 1396–1408. doi:10.1039/C9SE00787C.

[13] M.A. Arellano-Treviño, Z. He, M.C. Libby, R.J. Farrauto, Catalysts and adsorbents for CO_2 capture and conversion with dual function materials: Limitations of Ni-containing DFMs for flue gas applications, J. CO_2 Util. 31 (2019) 143–151. doi:10.1016/j.jcou.2019.03.009.

[14] C. Janke, M.S. Duyar, M. Hoskins, R. Farrauto, Catalytic and adsorption studies for the hydrogenation of CO_2 to methane, Appl. Catal. B Environ. 152–153 (2014) 184–191. doi:10.1016/j.apcatb.2014.01.016.

[15] Q. Zheng, R. Farrauto, A. Chau Nguyen, Adsorption and Methanation of Flue Gas CO_2 with Dual Functional Catalytic Materials: A Parametric Study, Ind. Eng. Chem. Res. 55 (2016) 6768–6776. doi:10.1021/acs.iecr.6b01275.

[16] C. Jeong-Potter, A. Porta, R. Matarrese, C.G. Visconti, L. Lietti, R. Farrauto, Aging study of low Ru loading dual function materials (DFM) for combined power plant effluent CO_2 capture and methanation, Appl. Catal. B Environ. 310 (2022) 121294. doi:10.1016/j.apcatb.2022.121294.

[17] E. García-Bordejé, A.B. Dongil, J. Moral, J.M. Conesa, A. Guerrero-Ruiz, I. Rodríguez-Ramos, Cyclic performance in CO_2 capture-methanation of bifunctional Ru with different base metals: Effect of the reactivity of CO_x ad-species, J. CO_2 Util. 68 (2023) 102370. doi:10.1016/j.jcou.2022.102370.

[18] Z. Kowalczyk, K. Stołecki, W. Raróg-Pilecka, E. Miśkiewicz, E. Wilczkowska, Z. Karpiński, Supported ruthenium catalysts for selective methanation of carbon oxides at very low CO_x/H_2 ratios, Appl. Catal. A Gen. 342 (2008) 35–39. doi:10.1016/j.apcata.2007.12.040.

[19] J.H. Kwak, L. Kovarik, J. Szanyi, CO_2 Reduction on Supported Ru/Al_2O_3 Catalysts: Cluster Size Dependence of Product Selectivity, ACS Catal. 3 (2013) 2449–2455. doi:10.1021/cs400381f.

[20] P. Panagiotopoulou, Hydrogenation of CO_2 over supported noble metal catalysts, Appl. Catal. A Gen. 542 (2017) 63–70. doi:10.1016/j.apcata.2017.05.026.

[21] Y. Yan, Q. Wang, C. Jiang, Y. Yao, D. Lu, J. Zheng, Y. Dai, H. Wang, Y. Yang, Ru/Al_2O_3 catalyzed CO_2 hydrogenation: Oxygen-exchange on metal-support interfaces, J. Catal. 367 (2018) 194–205. doi:10.1016/j.jcat.2018.08.026.

[22] S. Eckle, M. Augustin, H.-G. Anfang, R.J. Behm, Influence of the catalyst loading on the activity and the CO selectivity of supported Ru catalysts in the selective methanation of CO in CO_2 containing feed gases, Catal. Today. 181 (2012) 40–51. doi:10.1016/j.cattod.2011.08.035.

[23] X. Wang, Y. Hong, H. Shi, J. Szanyi, Kinetic modeling and transient DRIFTS–MS studies of CO2 methanation over Ru/Al_2O_3 catalysts, J. Catal. 343 (2016) 185–195. doi:10.1016/j.jcat.2016.02.001.

[24] S. Chen, A.M. Abdel-Mageed, M. Dyballa, M. Parlinska-Wojtan, J. Bansmann, S. Pollastri, L. Olivi, G. Aquilanti, R.J. Behm, Raising the CO_x Methanation Activity of a Ru/γ-Al_2O_3 Catalyst by Activated Modification of Metal–Support Interactions, Angew. Chemie - Int. Ed. 59 (2020) 22763–22770. doi:10.1002/anie.202007228.

[25] F. Goodarzi, M. Kock, J. Mielby, S. Kegnæs, CO_2 methanation using metals nanoparticles supported on high surface area MgO, J. CO_2 Util. 69 (2023) 102396. doi:10.1016/j.jcou.2023.102396.

[26] A. Quindimil, U. De-La-Torre, B. Pereda-Ayo, A. Davó-Quiñonero, E. Bailón-García, D. Lozano-Castelló, J.A. González-Marcos, A. Bueno-López, J.R. González-Velasco, Effect of metal loading on the CO_2 methanation: A comparison between alumina supported Ni and Ru catalysts, Catal. Today. 356 (2020) 419–432. doi:10.1016/j.cattod.2019.06.027.

[27] S. López-Rodríguez, A. Davó-Quiñonero, E. Bailón-García, D. Lozano-Castelló, A. Bueno-López, Effect of Ru loading on Ru/CeO_2 catalysts for CO_2 methanation, Mol. Catal. 515 (2021) 111911. doi:10.1016/j.mcat.2021.111911.

[28] S. Navarro-Jaén, J.C. Navarro, L.F. Bobadilla, M.A. Centeno, O.H. Laguna, J.A. Odriozola, Size-tailored Ru nanoparticles deposited over γ-Al_2O_3 for the CO_2 methanation reaction, Appl. Surf. Sci. 483 (2019) 750–761. doi:10.1016/j.apsusc.2019.03.248.

[29] A.M. Abdel-Mageed, K. Wiese, A. Hauble, J. Bansmann, J. Rabeah, M. Parlinska-Wojtan, A. Brückner, R.J. Behm, Steering the selectivity in CO_2 reduction on highly active Ru/TiO_2 catalysts: Support particle size effects, J. Catal. 401 (2021) 160–173. doi:10.1016/j.jcat.2021.07.020.

[30] Z. Kowalczyk, K. Stołecki, W. Raróg-Pilecka, E. Miśkiewicz, E. Wilczkowska, Z. Karpiński, Supported ruthenium catalysts for selective methanation of carbon oxides at very low CO_x/H_2 ratios, Applied Catalysis A: General 342 (2008) 35–39. doi.org/10.1016/j.apcata.2007.12.040.

[31] S. Cimino, F. Boccia, L. Lisi, Effect of alkali promoters (Li, Na, K) on the performance of Ru/Al_2O_3 catalysts for CO_2 capture and hydrogenation to methane, J. CO_2 Util. 37 (2020) 195–203. doi:10.1016/j.jcou.2019.12.010.

[32] Y. Guo, S. Mei, K. Yuan, D.-J. Wang, H.-C. Liu, C.-H. Yan, Y.-W. Zhang, Low-Temperature CO_2 Methanation over CeO_2 -Supported Ru Single Atoms, Nanoclusters, and Nanoparticles Competitively Tuned by Strong Metal–Support Interactions and H-Spillover Effect, ACS Catal. 8 (2018) 6203–6215. doi:10.1021/acscatal.7b04469.

[33] H.T.T. Nguyen, Y. Kumabe, S. Ueda, K. Kan, M. Ohtani, K. Kobiro, Highly durable Ru catalysts supported on CeO_2 nanocomposites for CO_2 methanation, Appl. Catal. A Gen. 577 (2019) 35–43. doi:10.1016/j.apcata.2019.03.011.

[34] S. López Rodríguez, A. Davó-Quiñonero, J. Juan-Juan, E. Bailón-García, D. Lozano-Castelló, A. Bueno-López, Effect of Pr in CO_2 Methanation Ru/CeO_2 Catalysts, J. Phys. Chem. C 2021, 125, 12038−12049. doi.org/10.1021/acs.jpcc.1c03539

[35] S. Cisneros, S. Chen, C. Fauth, A.M. Abdel-Mageed, S. Pollastri, J. Bansmann, L. Olivi, G. Aquilanti, H. Atia, J. Rabeah, M. Parlinska-Wojtan, A. Brückner, R.J. Behm, Controlling the selectivity of high-surface-area Ru/TiO_2 catalysts in CO_2 reduction - modifying the reaction properties by Si doping of the support, Appl. Catal. B Environ. 317 (2022) 121748. doi:10.1016/j.apcatb.2022.121748.

[36] A. Petala, P. Panagiotopoulou, Methanation of CO_2 over alkali-promoted Ru/TiO_2 catalysts: I. Effect of alkali additives on catalytic activity and selectivity, Appl. Catal. B Environ. 224 (2018) 919–927. doi:10.1016/j.apcatb.2017.11.048.

[37] S. Chen, A.M. Abdel-Mageed, M. Li, S. Cisneros, J. Bansmann, J. Rabeah, A. Brückner, A. Groß, R.J. Behm, Electronic metal-support interactions and their promotional effect on CO_2 methanation on Ru/ZrO_2 catalysts, J. Catal. 400 (2021) 407–420. doi:10.1016/j.jcat.2021.06.028.

[38] S. Abelló, C. Berrueco, F. Gispert-Guirado, D. Montané, Synthetic natural gas by direct CO_2 hydrogenation on activated takovites: effect of Ni/Al molar ratio, Catal. Sci. Technol. 6 (2016) 2305–2317. doi:10.1039/C5CY01200G.

[39] D. Wierzbicki, R. Baran, R. Dębek, M. Motak, M.E. Gálvez, T. Grzybek, P. Da Costa, P. Glatzel, Examination of the influence of La promotion on Ni state in hydrotalcite-derived catalysts under CO_2

methanation reaction conditions: Operando X-ray absorption and emission spectroscopy investigation, Appl. Catal. B Environ. 232 (2018) 409–419. doi:10.1016/j.apcatb.2018.03.089.

[40] P.H. Ho, G.S. de Luna, S. Angelucci, A. Canciani, W. Jones, D. Decarolis, F. Ospitali, E.R. Aguado, E. Rodríguez-Castellón, G. Fornasari, A. Vaccari, A.M. Beale, P. Benito, Understanding structure-activity relationships in highly active La promoted Ni catalysts for CO_2 methanation, Appl. Catal. B Environ. 278 (2020) 119256. doi:10.1016/j.apcatb.2020.119256.

[41] P.H. Ho, G. Sanghez de Luna, N. Schiaroli, A. Natoli, F. Ospitali, M. Battisti, F. di Renzo, C. Lucarelli, A. Vaccari, G. Fornasari, P. Benito, Effect of Fe and La on the Performance of NiMgAl HT-Derived Catalysts in the Methanation of CO_2 and Biogas, Ind. Eng. Chem. Res. 61 (2022) 10511–10521. doi:10.1021/acs.iecr.2c00687.

[42] D. Wierzbicki, R. Baran, R. Dębek, M. Motak, M.E. Gálvez, T. Grzybek, P. Da Costa, P. Glatzel, Examination of the influence of La promotion on Ni state in hydrotalcite-derived catalysts under CO_2 methanation reaction conditions: Operando X-ray absorption and emission spectroscopy investigation, Appl. Catal. B Environ. 232 (2018) 409–419. doi:10.1016/j.apcatb.2018.03.089.

[43] S. Xu, S. Chansai, Y. Shao, S. Xu, Y. Wang, S. Haigh, Y. Mu, Y. Jiao, C.E. Stere, H. Chen, X. Fan, C. Hardacre, Mechanistic study of non-thermal plasma assisted CO_2 hydrogenation over Ru supported on MgAl layered double hydroxide, Appl. Catal. B Environ. 268 (2020) 118752. doi:10.1016/j.apcatb.2020.118752.

[44] A. Ballarini, P. Benito, G. Fornasari, O. Scelza, A. Vaccari, Role of the composition and preparation method in the activity of hydrotalcite-derived Ru catalysts in the catalytic partial oxidation of methane, Int. J. Hydrogen Energ. 38 (2013) 15128-15139. doi.org/10.1016/j.ijhydene.2013.08.135.

[45] J J.A. Martins, A.C. Faria, M.A. Soria, C. V. Miguel, A.E. Rodrigues, L.M. Madeira, CO_2 Methanation over Hydrotalcite-Derived Nickel/Ruthenium and Supported Ruthenium Catalysts, Catalysts. 9 (2019) 1008. doi:10.3390/catal9121008.

[46] F. Cavani, F. Trifirò, A. Vaccari, Hydrotalcite-type anionic clays: Preparation, properties and applications., Catal. Today. 11 (1991) 173–301. doi:10.1016/0920-5861(91)80068-K.

[47] P. Betancourt, A. Rives, R. Hubaut, C.E. Scott, J. Goldwasser A study of the ruthenium-alumina system. Appl Catal A Gen 170 (1998) 307-314. doi.org/10.1016/S0926-860X(98)00061-1

[48] M. Wang, W. Weng, H. Zheng, X. Yi, C. Huang, H. Wan Oscillations during partial oxidation of methane to synthesis gas over Ru/Al_2O_3 catalyst. J. Nat. Gas. Chem. 18 (2009) 300-305. doi.org/10.1016/S1003-9953(08)60126-7.

[49] S.C.P. Maina, I. M. J. Vilella, A. D. Ballarini, S. Rubén de Miguel, Performance of Modified Alumina-Supported Ruthenium Catalysts in the Reforming of Methane with CO_2, Catalysts 13 (2023) 338. doi.org/10.3390/catal13020338.

[50] A. Infantes-Molina, J. Merida-Robles, E. Rodriguez-Castellon, J.L.G. Fierro, A. Jimenez-Lopez, Synthesis, characterization and catalytic activity of ruthenium-doped cobalt catalysts, Applied Catalysis A: General 341 (2008) 35–42. doi.org/10.1016/j.apcata.2007.12.034

[51] J.G. A. Batista Silva, R. Costa Santos, E. Rodríguez-Castellon, L.S. Gomes Teixeira, L.A. Magalhaes Pontes, Catalytic conversion of glucose into sorbitol over niobium oxide supported Ru catalysts, Molec. Catal. 507 (2021) 111567. https://doi.org/10.1016/j.mcat.2021.111567.

[52] J.J. Musci, M. Montaña, A.B. Merlo, E. Rodríguez-Aguado, J.A. Cecilia, E. Rodríguez-Castellon, I.D. Lick, M. L. Casella, Supported ruthenium catalysts for the aqueous-phase selective hydrogenation of furfural to furfuryl alcohol, Catalysis Today 394-396 (2022) 81–93. doi.org/10.1016/j.cattod.2021.12.011

[53] J.I. Di Cosimo, V.K. Díez, M. Xu, E. Iglesia, C.R. Apesteguía, Structure and surface and catalytic properties of Mg-Al basic oxides, J. Catal. 178 (1998) 499–510. doi:10.1006/jcat.1998.2161.

[54] Q. Pan, J. Peng, T. Sun, S. Wang, S. Wang, Insight into the reaction route of CO_2 methanation: Promotion effect of medium basic sites, Catal. Commun. 45 (2014) 74–78. https://doi.org/10.1016/j.catcom.2013.10.034.

[55] G. Garbarino, D. Bellotti, E. Finocchio, L. Magistri, G. Busca, Methanation of carbon dioxide on Ru/Al_2O_3: Catalytic activity and infrared study, Catalysis Today 277 (2016) 21–28. doi.org/10.1016/j.cattod.2015.12.010.

[56] J.A.H. Dreyer, P. Li, L. Zhang, G.K. Beh, R. Zhang, P.H.-L. Sita, W. Y. Teoh, Influence of the oxide support reducibility on the CO_2 methanation over Ru-based catalysts, Appl. Catal. B: Env. 219 (2017) 715–726. doi.org/10.1016/j.apcatb.2017.08.011

[57] O.D. Pavel, R. Zăvoianu, R. Bîrjega, E. Angelescu, V.I. Pârvulescu, Mechanochemical versus co-precipitated synthesized lanthanum-doped layered materials for olefin oxidation, Appl. Catal. A Gen. 542 (2017) 10–20. doi:10.1016/j.apcata.2017.05.012.

[58] M. Bailera, P. Lisbona, B. Peña, A. Alarón, J. Guilera, J. Perpíñan, L. M. Romeo, Synthetic natural gas production in a 1 kW reactor using $Ni\text{-}Ce/Al_2O_3$ and $Ru\text{-}Ce/Al_2O_3$: Kinetics, catalyst degradation and process design, Energy 256 (2022) 124720. doi.org/10.1016/j.energy.2022.124720.

Graphical abstract

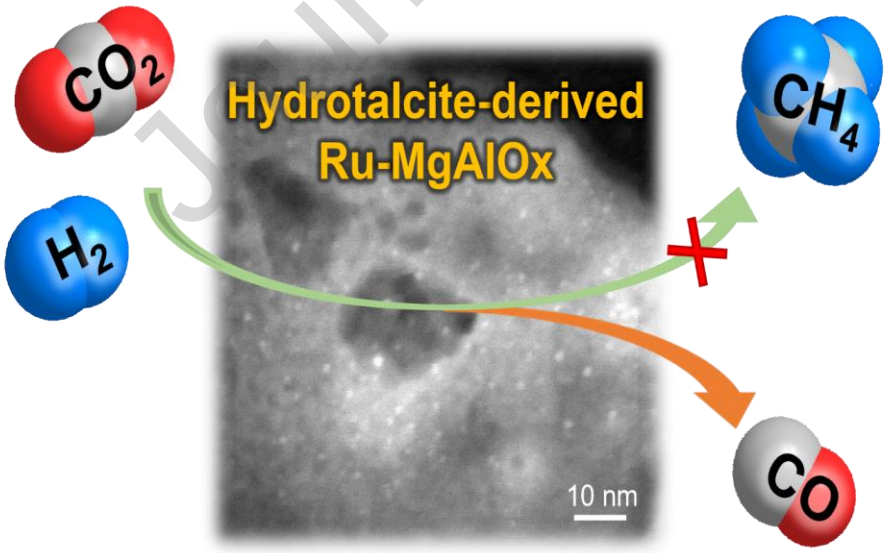

CRediT authorship contribution statement

Alexander Misol: Methodology, Investigation, Writing – original draft. **Ilenia Giarnieri**: Investigation. **Francesca Ospitali**: Measurements. **Adriana Ballarini:** Investigation, Validation, Writing – review & editing. **José Jiménez-Jiménez:** Investigation, Validation, Writing – review & editing. **Enrique Rodríguez-Castellón:** Investigation, Validation, Writing – original draft, Writing – review & editing, Funding acquisition. **Francisco Martín Labajos:** Investigation, Validation, Writing – review & editing. **Giuseppe Fornasari:** Investigation, Validation, Writing – review & editing. **Patricia Benito:** Conceptualization, Validation, Supervision, Writing – original draft, Writing – review & editing, Funding acquisition.

Declaration of interests

☒ The authors declare that they have no known competing financial interests or personal relationships that could have appeared to influence the work reported in this paper.

☐ The authors declare the following financial interests/personal relationships which may be considered as potential competing interests:

Highlights

- RuMgAl HT-derived catalysts for the valorization of CO_2.
- Small Ru nanoparticles finely dispersed in the $MgAlO_x$ matrix.
- The basicity of the support is modified by adding La^{3+}.
- The selectivity of the process is shifted to the production of CO.